Lab on a Chip

METHOD

View Article Online
View Journal | View Issue

Cite this: *Lab Chip*, 2015, **15**, 2140

Investigating the fluid dynamics of rapid processes within microfluidic devices using bright-field microscopy†

Tohid Pirbodaghi,[a] Daniele Vigolo,[b] Samin Akbari[c] and Andrew deMello*[b]

Received 12th February 2015,
Accepted 18th March 2015

DOI: 10.1039/c5lc00175g

www.rsc.org/loc

The widespread application of microfluidic devices in the biological and chemical sciences requires the implementation of complex designs and geometries, which in turn leads to atypical fluid dynamic phenomena. Accordingly, a complete understanding of fluid dynamics in such systems is key in the facile engineering of novel and efficient analytical tools. Herein, we present an accurate approach for studying the fluid dynamics of rapid processes within microfluidic devices using bright-field microscopy with white light illumination and a standard high-speed camera. Specifically, we combine Ghost Particle Velocimetry and the detection of moving objects in automated video surveillance to track submicron size tracing particles *via* cross correlation between the speckle patterns of successive images. The efficacy of the presented technique is demonstrated by measuring the flow field over a square pillar (80 μm × 80 μm) in a 200 μm wide microchannel at high volumetric flow rates. Experimental results are in excellent agreement with those obtained *via* computational fluid dynamics simulations. The method is subsequently used to study the dynamics of droplet generation at a flow focusing microfluidic geometry. A unique feature of the presented technique is the ability to perform velocimetry analysis of high-speed phenomena, which is not possible using micron-resolution particle image velocimetry (μPIV) approaches based on confocal or fluorescence microscopy.

Introduction

Since microfluidic devices have become increasingly popular tools in chemical and biological experimentation,[1–6] direct methods for elucidating the dynamics of fluid flow on the micron scale have similarly become central for their successful design and function. Micron-resolution Particle Image Velocimetry (μPIV) represents the state-of-the-art in the experimental quantification of such velocity flow fields.[7–13] In μPIV, a fluid is typically seeded with sub-micron fluorescent particles and illuminated using a pulsed laser light source to extract serial images of the particles over a specified time interval. Subsequently the particle positions over short time intervals are cross-correlated to infer the flow velocity field.[12] Particle Tracking Velocimetry (PTV) is a related technique where single particles are traced to determine their displacement within a moving fluid.[14–16] PTV is often called low particle density PIV because sparse seeding of particles is usually adopted to prevent particle misidentification and to allow individual particle tracking.[15] Despite their documented utility, both techniques require complex optical infrastructure such as confocal or fluorescence microscopy and pulsed laser source.[17–20]

Besides its application in PIV analysis, the detection of moving objects in a dynamic sense is a fundamental operation in video surveillance applications.[21–24] Here, a given frame of a video scene is compared with a static background frame, allowing moving objects to be identified by background subtraction.[24] Prior to application of an image correlation function, background subtraction is used to increase the accuracy of PIV data by improving the images of illuminated tracer particles on both macro[25–27] and micro[28] scales. Typically, the background static contribution is computed by averaging together all of the frames in a sequence. These techniques are however limited to steady flow conditions and further cannot accurately capture fast dynamic events such as droplet generation in microfluidic devices. An elegant refinement of the basic PIV methodology was recently introduced

[a] *Department of Mechanical Engineering, Massachusetts Institute of Technology, Cambridge, MA 02139, USA*
[b] *Institute of Chemical and Bioengineering, ETH Zurich, Vladimir Prelog Weg 1, 8093 Zurich, Switzerland. E-mail: andrew.demello@chem.ethz.ch*
[c] *Department of Chemical Engineering, Massachusetts Institute of Technology, Cambridge, MA 02139, USA*

† Electronic supplementary information (ESI) available: Supplementary Discussion, which includes a Materials and Methods section, a Supplementary Figure, and 5 Supplementary Movies. See DOI: 10.1039/c5lc00175g

by Buzzaccaro *et al.*[29] This so-called Ghost Particle Velocimetry (GPV) utilizes a standard bright field microscope to illuminate a sample containing sub-micron sized tracer particles. By controlling the numerical aperture of the condenser lens (in the illumination path) and by subtracting the static background contribution from each frame it is possible to record the speckle pattern generated by the interference of light scattered by the suspended tracers.[30] The speckle pattern is then used to evaluate the velocity of the fluid using a cross-correlation approach similar to that used in PIV and μPIV.

Herein, we apply the basic principles of GPV to study rapid phenomena within microfluidic systems and in the presence of moving boundaries. Specifically, we analyse the speckle pattern obtained from two consecutive images of a flow field seeded with 200 nm particles and illuminated by a white light source. Speckle patterns are obtained by subtracting out the median of several successive frames as the background static contribution, rather than using the averaging method adopted by Buzzaccaro *et al.* This approach has been proven to be more efficient and robust in detecting moving objects[24] and moreover enables analysis of a flow field with moving boundary conditions such as droplet generation within microfluidic devices.

Buzzaccaro *et al.* showed examples where they took advantage of the steady nature of their flows and averaged over several hundreds of frames to improve the statistics of the velocimetry data. Here, we extend their technique to the case of fast-happening phenomena in microfluidics and in the presence of moving boundary conditions. We obtain the speckle patterns by subtracting out the median of 10 to 20 successive frames as background static contribution instead of using the average as in Buzzaccaro *et al.* Using the median enables analysis of a flow field with moving boundary conditions like droplet generation in microfluidic devices, which was not addressed by Buzzaccaro *et al.*

Our experimental setup consists of a standard inverted bright field microscope (Ti-E, Nikon, Japan), white light illumination, and a high-speed camera (Phantom Miro M310, Vision Research, USA). To demonstrate the efficacy of the approach, the flow field over a square pillar (80 μm × 80 μm) within a microchannel (200 μm width and 50 μm height) was extracted and compared with CFD simulations using the COMSOL microfluidics module (COMSOL, Massachusetts, USA). We used COMSOL Multiphysics 4.4a to create a 2-D model using the laminar single-phase flow application mode of the microfluidic module. We performed a 2-D simulation because our experiments explore the flow velocity of 2-D plane located in the channel mid-plane. The density and viscosity were set to those of water at 25 °C, and flow was fully developed at the inlet with the boundaries (channel and pillar walls) set to the no slip boundary condition. The flow was allowed to exit passively at the outlet *via* a null pressure condition, *i.e.* $p = 0$.

Finally, the fluid dynamics of droplet generation at a flow focusing microfluidic geometry was investigated using the defined methodology.

Results and discussion

Flow over a rectangular pillar in a microchannel

Fig. 1(a) shows a bright-field image of a channel (200 μm wide and 50 μm high) containing a square pillar (80 μm × 80 μm) at its center. The microfluidic device was fabricated in polydimethylsiloxane (PDMS) using standard soft lithographic methods.[31]

A deionized (DI) water flow seeded with 200 nm polystyrene particles (0.05% by weight, Thermo Fisher Scientific, Molecular Probes FluoSpheres, USA) moves from left to right (at 10 μl min^{-1}) (Movie S1†). The median of 20 successive frames, shown in Fig. S1,† is sufficient to remove the effects of the static background contribution from each frame and reveal the speckle pattern generated by the moving particles (Fig. 1(b) and Movie S2†). The open-source PIVlab 1.32 MATLAB toolbox was used to cross correlate particle movement using speckle patterns from two successive images and thus derive the corresponding velocity field.[32] Fig. 2 provides a comparison of the experimentally determined flow velocity over the pillar within the microchannel with COMSOL simulation results. Comparison of the images clearly demonstrates the close correspondence between experimental data and theory. Importantly, using only standard laboratory equipment, the method is accurate, fast, and simple to implement, even for the high-speed flows typical in microfluidic environments (up to 0.5–2 m s^{-1}).

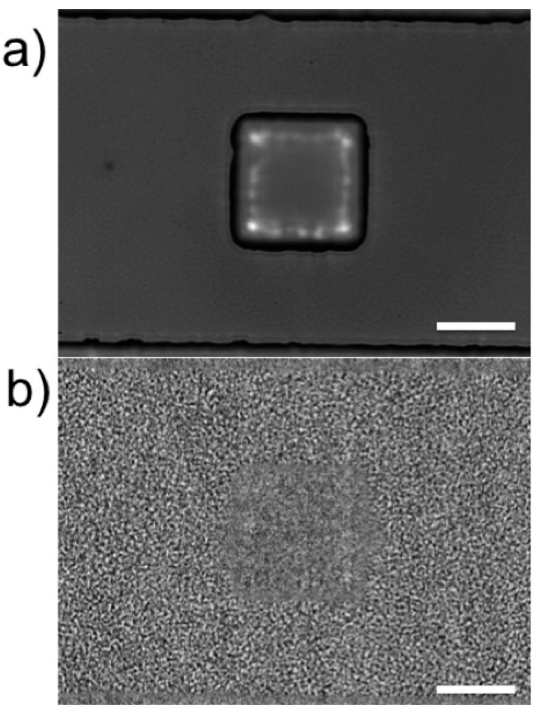

Fig. 1 (a) Bright field image of 200 nm polystyrene particles (concentration 0.05% by weight) dispersed in deionized water flowing through a microchannel containing a square pillar (80 μm × 80 μm). The average volumetric flow rate is 10 μl min^{-1} and the flow direction is from left to right. (b) Speckle pattern of the bright field image obtained by subtraction of the median image. Scale bars are 50 μm.

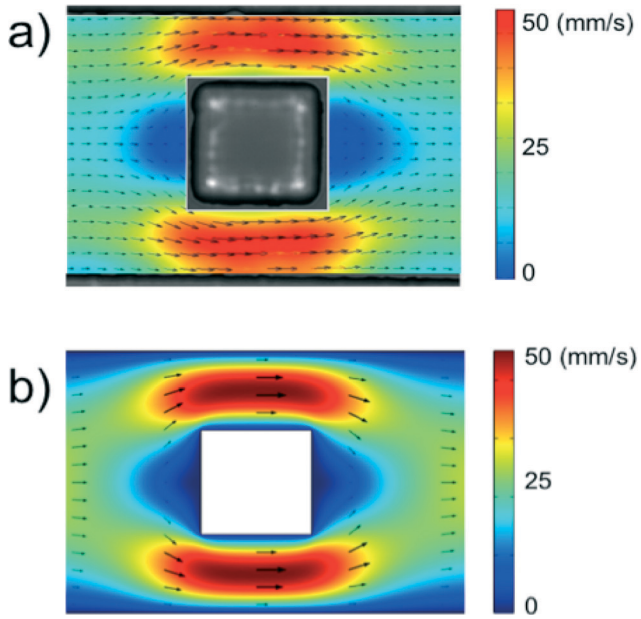

Fig. 2 Comparison of the flow velocity field around a 80 μm × 80 μm pillar within a microchannel obtained experimentally (a) and *via* a finite element simulation (b).

Dynamics of droplet generation

As a second example, we used the described protocol to study the dynamics of droplet generation at a flow focusing microfluidic geometry. Fluorinated oil (FC-40, Sigma, Poole, UK) and deionized water seeded with 200 nm polystyrene particles were used to generate water-in-oil droplets as shown in Fig. 3 (for further details, see ESI† and Movie S3).

Fig. 4 shows bright field images and the velocity distribution of the aqueous phase during necking but before breakup of a droplet at the channel mid-plane. As a finger of the aqueous phase extends into the junction and starts to neck, its velocity reaches the maximum value and a stagnation point develops at its tip as shown in Fig. 4. As the droplet grows, these two "high" and "low" velocity fields move toward each other and immediately before pinch off the stagnation point, which is located at the tip of the growing droplet moves to the center of droplet with two high velocity fields around it. Fig. 5 shows fluid movement inside a droplet moving within the channel immediately after pinch off. Velocities are relative to the coordinate system attached to the droplet at the channel mid-plane. The data illustrate two circulation zones that are hydrodynamically isolated from each other.[17]

As the droplet moves forward from right to left, the liquid–liquid interface drags the aqueous phase near to the interface because of the continuity of viscous stresses, as oil is more viscous than water. Since the droplet has a confined volume, the dragged fluid must move back through the droplet center.

Fig. 5 also demonstrates that there are four main stagnation points within the droplet moving in a channel relative to the coordinate system attached to the droplet. Two of the stagnation points are located outside of these circulation zones at the interface of oil and aqueous phases (right at the front and back of the droplet) and two of them are located in the center of circulation zones. The circulation zones and velocity field within the droplet moving in the channel are in very good agreement with previously published results.[17]

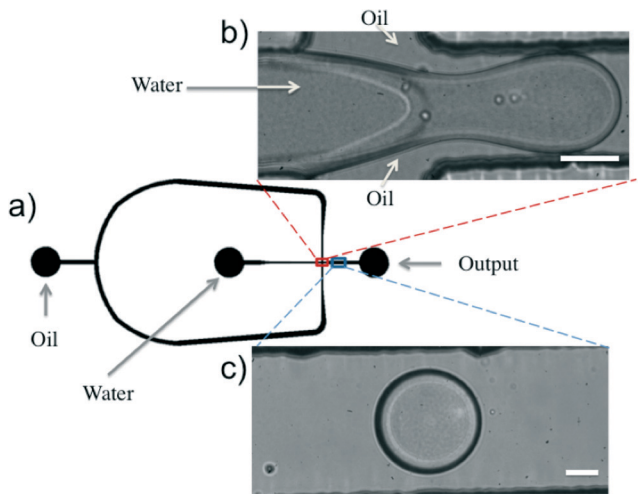

Fig. 3 Droplet generation at a flow focusing geometry. (a) The microfluidic device is made by standard soft-lithography in PDMS and contains rectangular cross-section channels with a height of 50 μm. To produce droplets, fluorinated oil (FC-40) containing 2% w/w surfactant is used as the continuous phase and deionized (DI) water seeded with 200 nm polystyrene particles as the dispersed phase (0.05% by weight). (b) Bright field image of drop formation at a generation rate of 600 Hz. (c) A bright field image of a droplet 300 microns downstream of the formation point. Scale bars are 25 μm. The focal plane considered is the mid-plane.

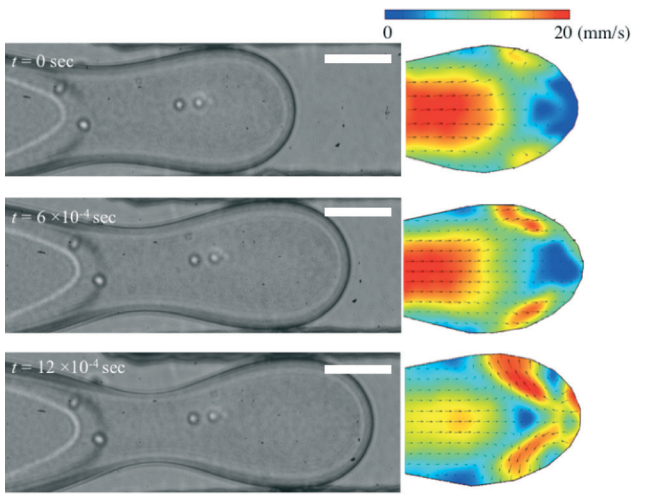

Fig. 4 (Left) Bright field images of an aqueous phase seeded with 200 nm polystyrene particles (0.05% by weight) necking in the drop making junction at time intervals of 600 μs and at the channel mid-plane prior to pinch-off. (Right) Comparison of the corresponding velocity distributions in the aqueous phase. Scale bars are 50 μm. The focal plane considered is the mid-plane.

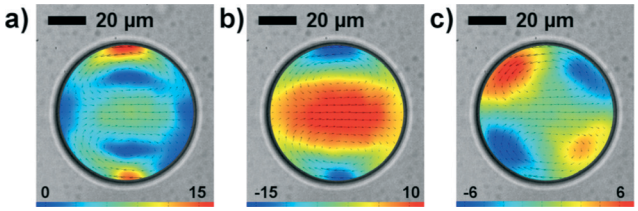

Fig. 5 a) Velocity distribution inside a droplet moving from right to left at a linear velocity of 55 mm s^{-1}. There are two circulation zones hydrodynamically isolated from each other inside the droplet, b) the velocity profile in the *x* direction, c) the velocity profile in the *y* direction. The focal plane considered is the middle plane. The aqueous droplet is seeded with 200 nm polystyrene particles (0.05% by weight).

Conclusions

We have presented a simple and direct approach for extracting velocimetry data from microfluidic environments and have demonstrated the accurate measurement of velocity fields with high spatial resolution. A key feature of the presented method is that it is equally applicable to unsteady fluid flows that possess moving boundary conditions. Moreover, the approach can provide a rapid estimation of fluid dynamics within microfluidic channels to aid component design. Importantly, the advantages introduced by this novel approach include its simplicity and ease of construction/operation. Indeed, in these proof-of-principle studies, we have investigated the fluid dynamics of droplet generation at a flow-focusing geometry as well as the internal flow of an enclosed droplet moving within a microchannel. The technique represents a cost-effective method in laboratories where fast camera setups are already available, and a reliable alternative to current μPIV approaches, which are limited by their sophisticated experimental setups, but also improves temporal resolution by exploiting bright field illumination and fast image acquisition. Finally, it should be noted that the basic method can be directly extended to the extraction of 3-D velocity fields.[17,24,29] Herein, the entire flow field is illuminated using a white light source. However, the objective focal planes can be adjusted in three-dimensional space *via* variation of the numerical aperture of the condenser lens (see discussion in the ESI†). Since, a controlled numerical aperture allows precise definition of measurement planes, 3-D velocity distributions over the entire flow domain can be constructed by stacking cross-sectional velocity fields at multiple focal planes using the continuity equation.

The ultimate limitations of the presented technique relate to the spatial accuracy and the frame rate recordable by the camera. While the latter, that limits the maximum velocity measurable, will be easily improved by advancements in fast camera technology, the first limitation is intrinsic to the method. In fact, each velocity value is obtained from the average of a region of interest (ROI) that has a finite area. The ROI should contain enough speckles to be able to correlate the speckle pattern of two consecutive frames and obtain a velocity vector. In our experimental setup we found the minimum ROI size to be about 7 × 7 μm^2, independently of the objective magnification used. This represents the spatial resolution limit of our technique.

Finally, in the experiments, we used up to 20 consecutive frames (captured at camera speeds of 10 000 frames per second) to extract the flow velocity field. Accordingly, it is safe to assume that we were able to capture phenomena that occur within 2 milliseconds. However, our camera can capture up to 100 000 fps, which enables us to study phenomena occurring within 0.2 milliseconds.

Acknowledgements

T. Pirbodaghi thanks the Swiss National Foundation (SNF) for the award of a post-doctoral fellowship (Number: 155481). D. Vigolo thanks the ETH Zurich Postdoctoral Fellowship Program and the Marie Curie Actions for People COFUND Program for partially supporting this project. The authors declare no competing financial interest.

References

1 S. Akbari and T. Pirbodaghi, *Lab Chip*, 2014, **14**, 3275–3280.
2 D. J. Beebe, G. A. Mensing and G. M. Walker, *Annu. Rev. Biomed. Eng.*, 2002, **4**, 261–286.
3 Z. H. Fan and D. J. Beebe, *Lab Chip*, 2014, **14**, 12–13.
4 A. M. Foudeh, T. Fatanat Didar, T. Veres and M. Tabrizian, *Lab Chip*, 2012, **12**, 3249–3266.
5 S. Akbari and T. Pirbodaghi, *Microfluid. Nanofluid.*, 2014, **16**, 773–777.
6 M. Kuhnemund, D. Witters, M. Nilsson and J. Lammertyn, *Lab Chip*, 2014, **14**, 2983–2992.
7 M. R. Bown, J. M. MacInnes and R. W. K. Allen, *Exp. Fluids*, 2007, **42**, 197–205.
8 C. Cierpka and C. J. Kähler, *J. Vis.*, 2012, **15**, 1–31.
9 C. D. Meinhart, S. T. Wereley and J. G. Santiago, *Exp. Fluids*, 1999, **27**, 414–419.
10 J. G. Santiago, S. T. Wereley, C. D. Meinhart, D. J. Beebe and R. J. Adrian, *Exp. Fluids*, 1998, **25**, 316–319.
11 V. van Steijn, M. T. Kreutzer and C. R. Kleijn, *Chem. Eng. Sci.*, 2007, **62**, 7505–7514.
12 S. T. Wereley and C. D. Meinhart, *Annu. Rev. Fluid Mech.*, 2010, **42**, 557–576.
13 S. Williams, C. Park and S. Wereley, *Microfluid. Nanofluid.*, 2010, **8**, 709–726.
14 T. Dracos, in *Three-Dimensional Velocity and Vorticity Measuring and Image Analysis Techniques*, ed. T. Dracos, Springer, Netherlands, 1996, vol. 4, ch. 7, pp. 155–160.
15 R. J. Adrian, *Annu. Rev. Fluid Mech.*, 1991, **23**, 261–304.
16 R. Lindken, M. Rossi, S. Große and J. Westerweel, Micro-particle image velocimetry (μPIV): recent developments, applications, and guidelines, *Lab Chip*, 2009, **9**(17), 2551–2567.
17 H. Kinoshita, S. Kaneda, T. Fujii and M. Oshima, *Lab Chip*, 2007, **7**, 338–346.

18 R. Lima, S. Wada, S. Tanaka, M. Takeda, T. Ishikawa, K.-I. Tsubota, Y. Imai and T. Yamaguchi, *Biomed. Microdevices*, 2008, **10**, 153–167.
19 J. Park, C. Choi and K. D. Kihm, *Exp. Fluids*, 2004, **37**, 105–119.
20 J. Raben, S. Klein, J. Posner and P. Vlachos, *Microfluid. Nanofluid.*, 2013, **14**, 431–444.
21 M. Cristani, M. Farenzena, D. Bloisi and V. Murino, *EURASIP J. Adv. Signal Process.*, 2010, 1–24.
22 R. Cucchiara, C. Grana, M. Piccardi and A. Prati, *IEEE Trans. Pattern Anal. Mach. Intell.*, 2003, **25**, 1337–1342.
23 R. Galicher, C. Marois, B. Macintosh, T. Barman and Q. Konopacky, *Astrophys. J., Lett.*, 2011, **739**, L41.
24 N. J. B. McFarlane and C. P. Schofield, *Mach. Vis. Appl.*, 1995, **8**, 187–193.
25 N. G. Deen, P. Willems, M. van Sint Annaland, J. Kuipers, R. G. Lammertink, A. J. Kemperman, M. Wessling and W. G. van der Meer, *Exp. Fluids*, 2010, **49**, 525–530.
26 M. Honkanen and H. Nobach, *Exp. Fluids*, 2005, **38**, 348–362.
27 R. Theunissen, F. Scarano and M. L. Riethmuller, *Exp. Fluids*, 2008, **45**, 557–572.
28 C. Zettner and M. Yoda, *Exp. Fluids*, 2003, **34**, 115–121.
29 S. Buzzaccaro, E. Secchi and R. Piazza, *Phys. Rev. Lett.*, 2013, **111**, 048101.
30 R. Cerbino and V. Trappe, *Phys. Rev. Lett.*, 2008, **100**, 188102.
31 D. C. Duffy, J. C. McDonald, O. J. A. Schueller and G. M. Whitesides, *Anal. Chem.*, 1998, **70**, 4974–4984.
32 W. Thielicke and E. J. Stamhuis, *J. Open Res. Software*, 2014, **2**(1), e30.

